ELSEVIER

NeuroImage

www.elsevier.com/locate/ynimg
NeuroImage 27 (2005) 436 – 441

Three-dimensional quantitative magnetisation transfer imaging of the human brain

Mara Cercignani,[a,*] Mark R. Symms,[b] Klaus Schmierer,[a] Philip A. Boulby,[b] Daniel J. Tozer,[a] Maria Ron,[a] Paul S. Tofts,[a] and Gareth J. Barker[c]

[a]*Department of Neuroinflammation, NMR Research Unit, 6th floor, University College London, Queen Square House, Institute of Neurology, Queen Square, London WC1N 3 BG, UK*
[b]*Department of Clinical and Experimental Epilepsy, Institute of Neurology, University College London, London WC1N 3BG, UK*
[c]*Centre for Neuroimaging Sciences, Department of Neurology, Institute of Psychiatry, Kings College London, London SE5 8AF, UK*

Received 7 January 2005; revised 1 April 2005; accepted 5 April 2005
Available online 22 June 2005

Quantitative magnetisation transfer (MT) analysis is based on a two-pool model of magnetisation transfer and allows important physical properties of the two proton pools to be assessed. A good signal-to-noise ratio (SNR) for the measured signal is essential in order to estimate reliably the parameters from a small number of samples, thus prompting the use of a sequence with high SNR, such as a three-dimensional spoiled gradient acquisition. Here, we show how full brain coverage can be accomplished efficiently, using a three-dimensional acquisition, in a clinically acceptable time, and without the use of large numbers of slice-selective radio-frequency pulses which could otherwise confound analysis. This acquisition was first compared in post mortem human brain tissue to established two-dimensional acquisition protocols with differing SNR levels and then used to collect data from six healthy subjects. Image data were fitted using the two pool model and showed negligible residual deviations. Quantitative results were assessed in several brain locations. Results were consistent with previous single-slice data, and parametric maps were of good quality. Further investigations are needed to interpret the regional variation of quantitative MT quantities.

Keywords: Structural MRI; Magnetisation transfer; White matter; Cross-relaxation

Introduction

The magnetisation transfer (MT) effect is based on the exchange of magnetisation occurring between protons in free water (the liquid pool) and those attached to larger molecules (the semisolid pool). By exploiting this exchange of magnetisation (Wolff and Balaban, 1989), it is possible to sensitise an MR experiment to the magnetic resonance characteristics of macromolecular protons by selective saturation. MT pulses can be applied to clinical imaging to improve the suppression of static tissue in MR angiography, to increase lesion conspicuity on conventional MRI, or to increase the visibility of enhancing lesions when gadolinium-based contrast agents are used (Silver et al., 1997). An MT weighted image can also be combined with an unweighted image to obtain the MT ratio (MTR).

Despite being a (semi-)quantitative measure, the MTR value is the result of the combination of several more fundamental quantities, and it is highly dependent on the acquisition parameters. Henkelman et al. (1993) developed a simple two-pool model for the quantitative interpretation of the MT phenomenon in gels, which allows these physical quantities – inaccessible by conventional means – to be estimated from a set of MT measurements. The application of quantitative MT in vivo has been pursued by other authors (Ramani et al., 2002; Sled and Pike, 2000, 2001; Sled et al., 2004; Tozer et al., 2003; Yarnykh, 2002), producing interesting results in healthy subjects (Sled et al., 2004), in patients with multiple sclerosis (Davies et al., 2004), and in those with tumours (Yarnykh, 2002).

Clinical applications of the technique are unfortunately still limited, mainly due to the long acquisition times and the limited brain coverage achievable. Since quantitative MT imaging requires the collection of a series of MT-weighted images and the estimation of a number of parameters by fitting a non-linear model to the measured signal, the acquisition time is predominantly affected by the number of data points required to achieve a sufficient signal-to-noise ratio (SNR) in the calculated maps. The number of data points can be decreased by reducing the number of model parameters to a subset, i.e. by imposing physically meaningful constraints on the others (Yarnykh and Yuan, 2004). This strategy has been shown to produce high-quality and high-resolution quantitative maps in healthy controls when used in combination with a 3D acquisition. While using a priori information to fix some of the model parameters can present several advantages in healthy tissues, the approach can be more

* Corresponding author. Fax: +44 207 278 5616.
E-mail address: m.cercignani@ion.ucl.ac.uk (M. Cercignani).
Available online on ScienceDirect (www.sciencedirect.com).

1053-8119/$ - see front matter © 2005 Elsevier Inc. All rights reserved.
doi:10.1016/j.neuroimage.2005.04.031

problematic in the presence of pathology, when the same quantities can vary independently in an unpredictable fashion. When no a priori hypotheses can be made, as many model parameters as possible should be fitted to the data, making the use of a pulse sequence with inherently high SNR even more important. This observation prompted us to evaluate the performance of different acquisition protocols.

In principle, data acquisition can use any pulse sequence, but due to their short scan times and low T_1 and T_2 contrast on unsaturated images, mainly single slice (Sled et al., 2004) or multislice (Davies et al., 2004; Tozer et al., 2003) 2D gradient echo (GE) sequences have been investigated to date. On the other hand, three-dimensional acquisitions overcome some of the limitations of multislice 2D GE acquisitions, such as interference between adjacent slices (Kucharczyk et al., 1988) and incidental MT effect from the slice-selective pulses used (Dixon et al., 1990). These advantages, the ability to provide whole brain coverage and the better SNR for a given time (Edelstein et al., 1986), have already led to 3D imaging being applied to (non quantitative) MT imaging and MTR measurement (Dousset et al., 1992; Finelli et al., 1996; Tanabe et al., 1998). A 3D pulse sequence was also used by Yarnykh and Yuan for their reduced quantitative MT model (Yarnykh and Yuan, 2004), allowing high-resolution maps to be produced.

In this report, we undertake a more complete analysis by implementing a time-efficient 3D spoiled gradient recalled echo (SPGR) sequence, which provides whole brain coverage and requires a relatively short acquisition time. This sequence allows the acquisition of more data for the MT model, permitting a more robust and complete fitting procedure and making the sequence suitable for clinical application. This 3D acquisition was validated in post mortem human brain tissue by comparing the estimated MT parameters with those obtained using a 2D acquisition. The sequence was also used to collect data from a group of healthy individuals, producing estimates of quantitative MT parameters in various brain locations.

Materials and methods

Background

This work is based on the simplified model of quantitative MT developed by Ramani et al. (2002). In brief, the Henkelman et al. (1993) model was modified by introducing f, the macromolecular proton fraction, as:

$$f = \frac{M_0^B}{M_0^B + M_0^A}, \tag{1}$$

where M_0^A and M_0^B are the fully relaxed values of magnetisation associated with the free pool, A, and the semisolid pool, B respectively. Using f, the MT-weighted signal intensity (S) can be written as:

$$S = gM_0^A \left(\frac{R_B \left[\frac{RM_0^A f}{R_A(1-f)} \right] + R_{RFB} + R_B + RM_0^A}{\left[\frac{RM_0^A f}{R_A(1-f)} \right](R_B + R_{RFB}) + \left(1 + \left[\frac{\omega}{2\pi\Delta f} \right]^2 \left[\frac{1}{R_A T_2^A} \right] \right)(R_{RFB} + R_B + RM_0^A)} \right). \tag{2}$$

In this equation, g is a scanner-dependent scaling factor, R is the MT exchange rate between the two pools; R_A (=$1/T_1^A$) and R_B are the longitudinal relaxation rates of the free and semi-solid pools respectively, and T_2^A is the transverse relaxation time of pool A. R_{RFB} represents the rate of loss of longitudinal magnetisation due to the irradiation by the MT pulse of amplitude ω, expressed in rad s^{-1}, and offset frequency Δf. R_{RFB} depends on the transverse relaxation time of the semisolid pool, T_2^B and, in brain tissue, it can be modelled assuming a super-Lorentzian lineshape (Li et al., 1997; Sled and Pike, 2000). For in vivo applications, ω can be estimated as the continuous wave power equivalent (CWPE), where the pulse is simply replaced by a continuous wave irradiation with the same mean square amplitude (Ramani et al., 2002). Only 6 independent parameters can be determined from Ramani's model: RM_0^A, gM_0^A, R_B, f/R_A $(1-f)$, $1/R_A T_2^A$, and T_2^B (Ramani et al., 2002). In order to extract f from the fitted f/R_A $(1-f)$, knowledge of R_A is also required. This can be achieved by measuring independently the observed longitudinal relaxation rate of the sample, R_{Aobs} (=$1/T_{1obs}$) (Henkelman et al., 1993). R_A can then be estimated according to the following relationship (Ramani et al., 2002):

$$R_A = \frac{R_{Aobs}}{1 + \frac{RM_0^A f}{R_A(1-f)} \frac{(R_B - R_{Aobs})}{R_B - R_{Aobs} + RM_0^A}}. \tag{3}$$

Pulse sequence and fitting routine

All images were obtained on a 1.5 T clinical scanner (SIGNA Horizon Echospeed, General Electric, Milwaukee, WI, USA).

The pulse sequence consists of a MT-weighted 3D fast SPGR acquisition with a TR of 30.7 ms and a TE of 5.3 ms. In order to minimise the amount of T1-weighting, an excitation flip angle of 5° was used. MT saturation was achieved using Gaussian pulses (standard deviation = 2.98 ms, duration = 14.6 ms), applied once every TR prior to RF excitation. Their flip angle and offset frequency were varied. Ten MT points were collected in total, for each of the experiments described below, using only two MT pulse powers, following the observations of Sled and Pike (2000) (the powers can be described by their equivalent on-resonance flip angles: low flip angle = 212° and high flip angle = 843°). For each power, five different frequency offsets, ranging from 400 Hz to 20000 Hz, were used. The frequencies were separated by a constant logarithmic step of about 0.4. For all the experiments reported in this paper, a matrix of 256 × 96 × 32 over a FoV of 240 × 180 × 160 mm^3 was used, for a total scan time of approximately 15 min. Data were then reconstructed to an in-plane matrix of 256 × 256 over a 24 × 24 cm FoV, while the 32 through-plane phase encode steps were used to reconstruct twenty-eight 5-mm-thick slices (with 4 slices being discarded to minimise wrap around effects). The manufacturer's birdcage head coil was used for both signal transmission and reception. The specific absorption rate (SAR) was estimated during scan setup, using the manufacturer's standard calculation routines, assuming a 'worst case scenario' of MT pulses with the maximum flip angle for all measurements; in no cases were the SAR limits reached or exceeded (runtime hardware SAR monitoring is provided as standard, for all sequences, by the scanner).

All image processing was performed on a Unix workstation (Sun Microsystems, Mountain View, CA, USA). The quantitative MT parameters were obtained as follows. Five of the six independent parameters of Eq. (2) (RM_0^A, gM_0^A, f/R_A $(1-f)$, $1/$

$R_A T_2^A$, and T_2^B) were estimated by fitting Ramani's model to the data, using the Levenberg–Marquardt method, as implemented in Numerical Recipes (Press et al., 1992). In order to correct the nominal flip angle of the MT pulses, the B_1 field was estimated using a calibration oil-filled phantom (24 cm diameter, 40 cm length), according to the method of Barker et al. (1998); the MT pulse nominal flip angle was then scaled by a factor equal to $B_{1\text{actual}}/B_{1\text{nominal}}$, where $B_{1\text{nominal}}$ is the B_1 field in the centre of the phantom. This correction was performed only for in vivo data. ω_{CWPE} was then calculated as described by Ramani et al. (2002). Look-up tables were used for the super-Lorentzian lineshape and its derivative in order to speed up the computation. R_B was set arbitrarily to 1 s^{-1} and kept fixed during the fitting, an approach adopted by other authors (Ramani et al., 2002; Sled and Pike, 2001; Tozer et al., 2003) because estimates of the other parameters are largely insensitive to the value of R_B, and R_B tends to vary widely during the fitting procedure, leading to physically meaningless estimates.

Validation of the technique

In order to validate the 3D acquisition against an established 2D protocol and to compare performance, a coronal post mortem brain slice (thickness: 1 cm) from one hemisphere of a patient with multiple sclerosis was scanned using two different protocols. The specimen was provided by the UK Multiple Sclerosis Tissue Bank, (Charing Cross Hospital, Imperial College London, London, UK). Age at death and disease duration were 44 and 18 years respectively. The sample was fixed for 133 days in 10% formalin solution. The following scans were collected during a single session: (a) the MT-weighted 3D-SPGR sequence, as described in the previous section, and (b) an MT-weighted 2D-SPGR sequence (TE/TR = 12/1040 ms, imaging flip angle = 25°, matrix = 256 × 96, NEX = 0.75, in plane FOV = 240 × 180, 28 5-mm-thick slices). For protocol (b), the same number of points (10, for a scan time of about 14 min) was collected using Gaussian MT pulses with the same duration and standard deviation as those used for protocol a) (14.6 and 2.98 ms, respectively). The flip angles of the MT pulses were chosen to be similar in the two protocols, within the constraints of their different interval between subsequent pulses (although this match was not perfect due both to differences in the CWPE and to the different handling of pulse scaling (Tofts et al., in press)). The same values of frequency offset per flip angle were used for both 2D and 3D acquisitions. All images were collected in the coronal plane. In order to compare the two protocols at similar SNR levels, protocol (b) was repeated 3 times for averaging purposes.

Four circular regions of interest (ROIs) (area = 13.2 mm^2) were placed on the unsaturated image of the post mortem brain slice, within the normal appearing white matter (NAWM), using a high resolution scan of the same slice as visual reference and carefully avoiding contamination with MRI-visible MS lesions, CSF and grey matter. The location of the ROIs is shown in Fig. 1i. Ten data points for each ROI were obtained by superimposing the ROI outlines on the 10 different MT-weightings available for each of the following: (1) the 3D data sets (3D), (2) a single 2D data set (2D), (3) the (magnitude) average of two 2D data sets (2D2AV), and (4) the (magnitude) average of three 2D data sets (2D3AV). The calculated ω_{CWPE} was, respectively, ω_{CWPE} = 212 and 845 rad s^{-1} for protocol (a); and ω_{CWPE} = 190 and 440 rad s^{-1} for protocol (b). For each ROI, the quantitative MT parameters were estimated using the fitting routine described previously.

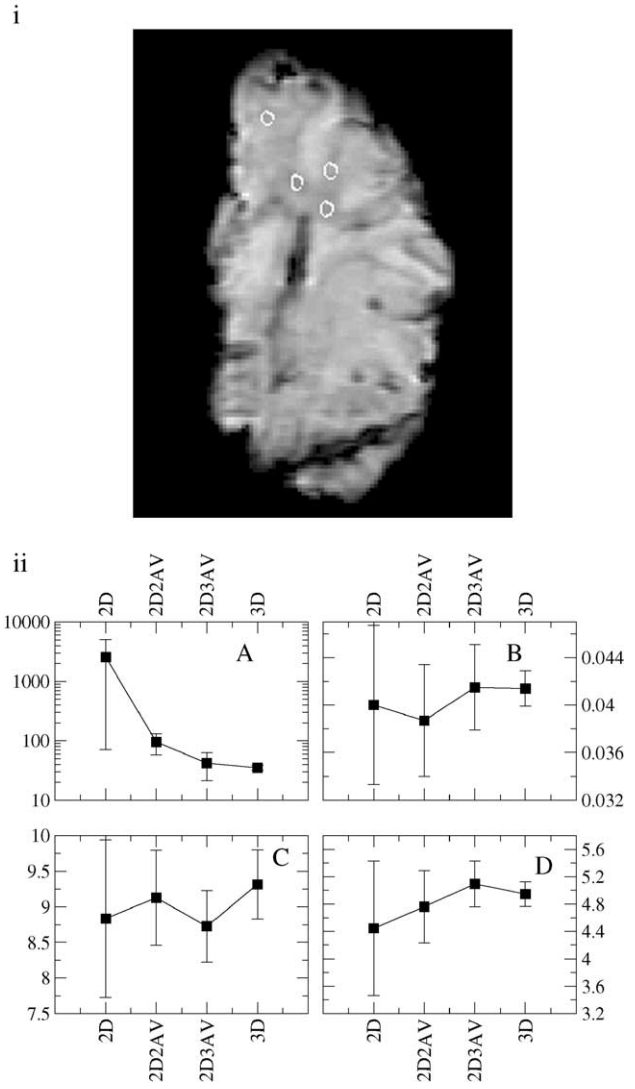

Fig. 1. (i) Location of the regions of interest on the post mortem slice; (ii) mean (squares) and standard error (bars) over the 4 regions for the MT parameters (A: RM_0^A, units of s^{-1}; B: f/[$R_A(1-f)$], units of s^{-1}; C: T_2^B, units of μs; D: 1/($R_A T_2^A$), units of s^{-2}). The abscissa represents the raw data type: 2D data set, the average of two 2D data sets, the average of three 2D data sets, and a 3D data set. See text for details.

In vivo MRI acquisition

Six healthy subjects (F/M = 2/4, mean age = 38.5 years, SD = 8.3 years) were scanned using the following protocol: (A) the 3D-MTSPGR acquisition described above; and (B) three 3D SPGR volumes (TR = 13.1 ms, TE = 4.2 ms) with three different excitation flip angles (α = 25°, 15°, 5°) in order to independently estimate the longitudinal relaxation rate of the system, R_{Aobs}. All images were collected along the axial plane. The same acquisition matrix and FoV as the MT-SPGR were used for sequence (B). The total imaging time was less than 20 min.

One subject (female, age 31 years) was scanned twice, the second time acquiring all the images in the coronal plane, with a protocol otherwise identical to the axial acquisition, to allow orientation and slice thickness dependant effects to be investigated.

The study was approved by the Joint Research Ethics Committee of The National Hospital for Neurology and the Institute of Neurology, UCL, and all subjects gave written informed consent before entering the study.

Image post-processing

For the in vivo data, the ten MT-weighted volumes obtained with sequence (A) and the three volumes obtained with sequence (B) were co-registered with the first MT-weighted volume using a modified (Symms et al., 2003) version of Automated Image Registration (AIR, available at http://air.bmap.ucla.edu:16080/AIR) (Woods et al., 1998). T_{1obs} was estimated on a pixel-by-pixel basis by fitting the theoretical SPGR signal equation to the SPGR signal (sequence B), as a function of the flip angle (Venkatesan et al., 1998). The nominal flip angle was corrected for B_1 inhomogeneities using the same method described for quantitative MT parameters (Barker et al., 1998). Quantitative MT parameters were estimated on a pixel-by-pixel basis as described in the previous section. Once the parameters had been estimated, R_A was computed using Eq. (3), f was extracted from the estimate of f/R_A $(1-f)$, and T_2^A was derived from the estimate of $1/R_A T_2^A$. Values of T_{1obs}, f, T_2^A, T_1^A, and T_2^B were measured by placing regions of interest (ROIs) on the T_1-weighted (flip angle = 25°) scans obtained from sequence (B) in various areas of white and grey matter (see Table 1). ROI outlines were then superimposed on the quantitative MT parametric maps, and the mean values were computed.

In order to investigate the effects of partial volume on the parameters measured in vivo, values obtained from the axial scan were pair wise compared with those obtained from the coronal scan in several ROIs.

Statistical correlations were assessed using the Spearman correlation coefficient in SPSS (SPSS Inc., Chicago, USA). All reported significances are two-tailed.

Results

Validation of 3D acquisition and SNR-related variability post mortem

The SNR of post mortem data was calculated as SNR = $S_{(NAWM)}/\sigma_{(NOISE)}$, where $S_{(NAWM)}$ is the average signal intensity measured in the ROIs on the image with the least amount of direct saturation (Δ = 20 kHz, ω_{CWPE} = 212 rad s^{-1} for the 3D acquisition, and ω_{CWPE} = 190 rad s^{-1} for the 2D acquisition), and $\sigma_{(NOISE)}$ is estimated on the same data by measuring the standard deviation of signal intensity in a region of background and dividing that value by 0.66, according to the method of Henkelman (1985). The resulting values were SNR2D (1 average) ≈43 and SNR3D ≈71, respectively. The mean values and the standard error for RM_0^A, f/R_A $(1-f)$, $1/R_A T_2^A$, and T_2^B obtained by fitting the model to the 4 data sets (2D, 2D2AV, 2D3AV, and 3D) are shown in Fig. 1ii (gM_0^A depends on an arbitrary multiplicative gain factor and therefore was not compared). The quantitative MT parameters obtained from the 4 data sets can be considered equivalent, within the experimental error. All estimates obtained from 2D data sets approach the values obtained from the 3D data sets when the number of averages and thus the SNR are increased. As expected, the standard error is also reduced when the number of averages is increased.

Table 1
Average quantitative MT parameters from the 3D-MTSPGR sequence, measured in the brain of six healthy volunteers

Area			f [%]	T_2^B [μs]	T_1^A [ms]	T_{1obs} [ms]	T_2^A [ms]
Corpus callosum	Genu	Mean	10.1	11.4	726	728	56.7
		SD	0.8	0.8	68	68	10.2
	Splenium	Mean	9.7	11.9	711	713	73.0
		SD	1.2	0.4	83	83	43.4
	Body	Mean	8.0	11.4	853	854	58.3
		SD	0.8	1.0	74	74	18.5
Internal capsule	Genu	Mean	9.0	12.7	749	751	54.8
		SD	1.2	1.2	67	67	12.7
	Posterior limb	Mean	9.3	13.8	734	736	56.7
		SD	1.1	8.9	47	47	4.9
Corona radiata		Mean	8.8	13.7	730	732	66.2
		SD	0.7	7.9	46	46	7.8
Optic radiation		Mean	9.4	12.3	661	663	61.1
		SD	0.9	8.4	44	44	7.7
Pedunculus cerebri		Mean	9.2	13.4	745	747	72.5
		SD	1.3	0.9	61	60	29.9
Cerebellar WM		Mean	9.4	11.8	718	719	59.0
		SD	0.8	0.5	51	51	3.8
Pons		Mean	8.1	11.7	825	827	77.3
		SD	0.9	1.1	70	70	17.3
Frontal WM		Mean	9.1	13.4	719	720	53.5
		SD	0.6	0.8	41	40	5.0
Thalamus		Mean	6.6	11.8	975	976	69.8
		SD	0.7	0.8	61	61	8.5
Caudate		Mean	5.0	11.4	1164	1164	82.8
		SD	0.6	0.8	117	117	19.0
Putamen		Mean	5.2	10.9	1092	1092	78.6
		SD	0.7	0.6	85	85	9.9
Frontal GM		Mean	4.7	11.8	1279	1279	107.6
		SD	0.6	1.6	128	128	26.2

f = macromolecular proton fraction; A = free pool; B = restricted pool; SD = standard deviation; GM = grey matter; WM = white matter. See text for further details.
With the exception of the corpus callosum and the pons, the values were measured bilaterally.

Whole-brain 3D acquisition in vivo

All in vivo images obtained with the 3D-MTSPGR were of good quality. The average SNR on the least saturated image, measured using a ROI positioned in the periventricular white matter, was 108.1. Typical parametric maps are shown in Fig. 2.

The fit of the MT-weighted signal intensity for two ROIs (40 voxels) is shown in Fig. 3. The variance of the fit (calculated as the sum of the squared difference between the data and the model, divided by the number of degrees of freedom) was 1.7 for the internal capsule (Fig. 3A) and 2.6 for the thalamus (Fig. 3B). The mean residual errors for these fits were 1.1% and 1.2%, respectively.

Average values for the estimated T_{1obs}, f, T_2^A, T_1^A, and T_2^B in various brain regions are summarised in Table 1.

Bivariate correlations (Spearman rank correlation coefficient) between parameters established a strong inverse correlation between T_1^A and f ($R = -0.9$, $P < 0.001$) and between T_2^A and f ($R = -0.7$, $P < 0.001$). T_1^A and T_2^A were also correlated, more strongly in grey matter ($R = 0.7$, $P < 0.001$) than in white matter ($R = 0.4$, $P < 0.001$). Paired samples correlations between parameters measured on axial and coronal acquisitions were,

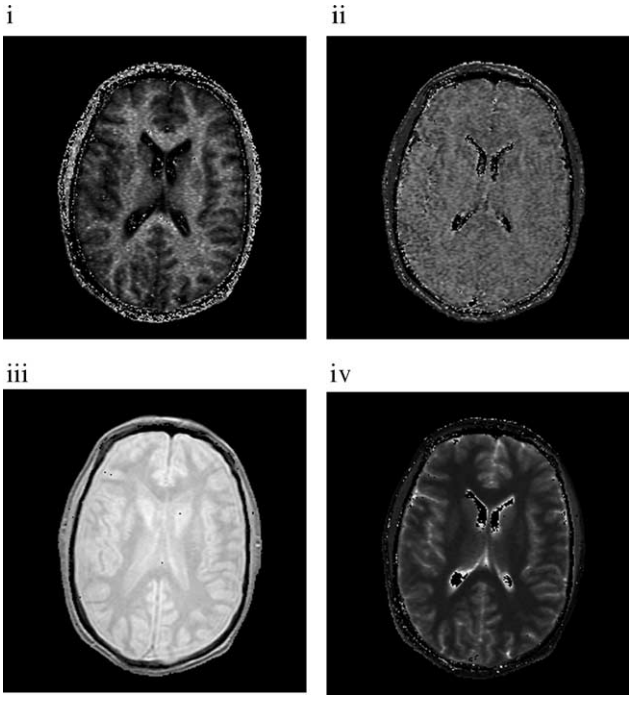

Fig. 2. Typical quantitative MT parametric maps obtained from a healthy subject using the 3D-MTSPGR acquisition described in the paper: macromolecular proton fraction, f (i); transverse relaxation time of the semisolid pool, T_2^B (ii); proton density, gM_0^A (iii); and longitudinal relaxation time of the free pool, T_1^A (iv).

respectively, 0.7 ($P < 0.001$) for f, 0.7 ($P < 0.001$) for T_1^A, 0.6 ($P = 0.003$) for T_2^B and 0.6 ($P = 0.003$) for T_2^A.

Discussion

A report describing regional variations of quantitative MT parameters within the brain of healthy subjects has recently been published, where a single 7-mm-thick slice was acquired (Sled et al., 2004). In the present study, the application of a 3D-MTSPGR sequence for quantitative MT acquisition allowed us to extend these investigations to a larger number of anatomical locations by collecting data from 6 healthy subjects, covering the whole brain with a $1 \times 2 \times 5$ mm^3 resolution in less than 20 min.

Whole-brain coverage can also be achieved using a 2D multislice acquisition (Davies et al., 2004; Tozer et al., 2003). However, a 3D Fourier encoding provides considerable advantages over a 2D multislice method, including improved SNR for comparable resolution and a reduction of partial volume effects and slice profile artefacts. Moreover, when using a 2D multislice acquisition, the incidental MT effect produced by subsequent slice excitation (Dixon et al., 1990) should be taken into account in modelling the signal intensity, particularly since this effect can vary with slice location.

In order to validate the 3D-MTSPGR acquisition, we have compared the performance of 2D and 3D SPGR in a post mortem brain slice. As expected, the SNR estimated on experimental data was higher for the 3D acquisition (despite the reduced excitation flip angle). The comparison was therefore carried out using 2D data sets characterised by different levels of SNR, obtained by averaging.

This analysis confirmed that quantitative MT could benefit from the use of a pulse sequence with high inherent SNR. Particularly, while the mean estimated value of $1/R_A T_2^A$ is very consistent across the 4 data sets, the other parameters appear more sensitive to raw data uncertainty.

Above all, RM_0^A tends to vary widely, even at high SNR. This is not surprising, as the measured signal is quite insensitive to variation in M_0^A (Graham and Henkelman, 1997), and in previous studies based on Ramani's model (Ramani et al., 2002), RM_0^A could not be estimated, as the fitting algorithm converged to large indiscriminate values. It has been argued that this parameter is highly sensitive to the timing of the pulse sequences; hence, its sensitivity to noise can be reduced by more accurate mathematical models (Yarnykh and Yuan, 2004). It is possible that the CWPE approximation is an oversimplification and that more sophisticated models may be required in order to accurately estimate the exchange rate between the two pools. Fortunately, the uncertainty in RM_0^A does not appear to affect the fit of the remaining parameters.

In terms of validating the 3D acquisition, the analysis of post mortem data showed that 2D and 3D acquisitions for quantitative MT produce consistent estimated quantitative MT parameters, in agreement within the confidence limits, particularly when several 2D data sets are averaged to reach an SNR comparable to the 3D data.

In vivo, the quantitative MT parametric maps obtained using the 3D-MTSPGR were characterised by acceptable quality; they appear visually slightly noisier than those published by Sled and Pike (2001), as would be expected given the smaller number of points (10 vs. 60) and the higher resolution used for the present study.

Quantitatively, all estimated parameters are within the range of expected values. Our average, T_2^B values show very good agreement with previously published data (Sled et al., 2004; Davies et al., 2004). Interestingly, this parameter is characterised by a significant variability within white matter, which may result from different fibre geometries in different areas of the brain. The highest values were measured in the internal capsule, corona radiata, and pedunculus cerebri, and the lowest in the corpus callosum and in the

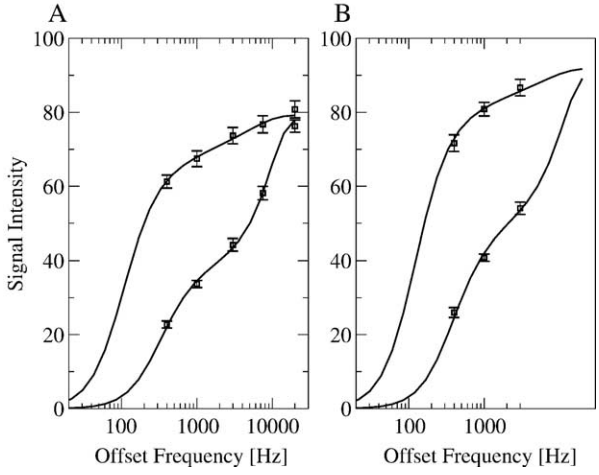

Fig. 3. Typical curves obtained by fitting the 10 MT-weighted mean signal intensities (squares) measured in manually drawn regions positioned in the posterior limb of the left internal capsule (A) and in the right thalamus (B). The error bars show the standard deviation of signal intensity (arbitrary units) within the region. The residual error was 1.1% for the internal capsule and 1.2% for the thalamus.

pons. The explanation for this finding is unclear. Since the resolution of the parametric maps is higher in-plane than in the slice-selective direction, the partial volume with either grey matter or CSF could affect T_2^B estimates in white matter fibres running within the axial plane, while preserving those running in the superior–inferior direction. However, the distribution of T_2^B estimated from a coronal data set showed a similar trend to those obtained from an axial data set, suggesting that the observed T_2^B variation does not originate from a partial volume artefact.

Yarnykh and Yuan (2004) imposed a fixed value to T_2^B and therefore found no spatial variation of this parameter; however, they did note a variation in f maps with position when using an acquisition with thinner slices than ours. This was explained as a result of the variable density of myelinated fibres in white matter tracts. The reason why the underlying structure is reflected by two different parameters in the two different studies is unclear, but it might be related to the use of different MT models in the two studies. Particularly, since Yarnykh and Yuan fitted a reduced model (with fixed T_2^B) to their experimental data, it is conceivable that the variation in T_2^B was reflected by a different parameter. Despite these differences, this result confirms that quantitative MT is sensitive to white matter architecture.

Provided that differences in the model are taken into account, the f values in our study are consistent with those obtained in an earlier study (Sled et al., 2004). Here, we used the relation $f = F / (1 + F)$ when comparing previously published values of the relative size of the restricted pool to f, where $F = M_0^B / M_0^A$.

For the present proof of concept study, we used a simplistic approach for correcting the nominal flip angles of the MT pulses. Clearly, the use of calibration scans on a phantom to estimate the B_1 field is not ideal since field homogeneity may vary due to loading or standing wave effects. Nevertheless, such effects should be subtle, and we have evidence from the phantom measurements that the birdcage head coil we used gives very high homogeneity over its normal imaging volume. For future clinical applications of the quantitative MT protocol here described, particularly at higher field strength, a direct measure of B_1 uniformity in the head should be obtained at the acquisition time.

References

Barker, G.J., Simmons, A., Arridge, S.R., Tofts, P.S., 1998. A simple method for investigating the effects of non-uniformity of radio-frequency transmission and radiofrequency reception in MRI. Br. J. Radiol. 71, 59–67.

Davies, G.R., Tozer, D.J., Cercignani, M., Ramani, A., Dalton, C.M., Thompson, A.J., Barker, G.J., Tofts, P.S., Miller, D.H., 2004. Estimation of the macromolecular proton fraction and bound pool T2 in multiple sclerosis. Mult. Scler. 10, 607–613.

Dixon, W.T., Engels, H., Castillo, M., Sardashti, M., 1990. Incidental magnetization contrast in standard multislice imaging. Magn. Reson. Imaging 8, 417–422.

Dousset, V., Grossman, R.I., Ramer, K.N., Schnall, M.D., Ypung, L.H., Gonzales-Scarano, F., Lavi, E., Cohen, J.A., 1992. Experimental allergic encephalomyelitis and multiple sclerosis: lesion characterisation with magnetization transfer imaging. Radiology 182, 483–491.

Edelstein, W.A., Glover, G.H., Hardy, C.J., Redington, R.W., 1986. The intrinsic signal-to-noise ratio in NMR imaging. Magn. Reson. Med. 3, 604.

Finelli, D.A., Hurst, G.C., Amantia Jr., P., Gullapali, R.P., Apicella, A., 1996. Cerebral white matter: technical development and clinical applications of effective magnetization transfer (MT) power concepts for high power, thin section, quantitative MT examinations. Radiology 199, 219–226.

Graham, S.J., Henkelman, R.M., 1997. Understanding pulsed magnetization transfer. J. Magn. Reson. Imaging 7, 903–912.

Henkelman, R.M., 1985. Measurement of signal intensities in the presence of noise in MR images. Med. Phys. 12, 232–233.

Henkelman, R.M., Huang, X., Xiang, Q.S., Stanisz, G.J., Swanson, S.D., Bronskill, M.J., 1993. Quantitative interpretation of magnetization transfer. Magn. Reson. Med. 29, 759–766.

Kucharczyk, W., Crawley, A.P., Kelly, W.M., Henkelman, R.M., 1988. Effect of multislice interference on image contrast in T2- and T1-weighted MR images. Am. J. Neuroradiol. 9, 443–451.

Li, J.G., Graham, S.J., Henkelman, R.M., 1997. A flexible magnetization transfer line shape derived from tissue experimental data. Magn. Reson. Med. 37, 866–871.

Press, W.H., Teukolsky, S.A., Vettering, W.T., Flannery, B.P., 1992. Numerical Recipes in C. Cambridge University Press, pp. 681–688.

Ramani, A., Dalton, C., Miller, D.H., Tofts, P.S., Barker, G.J., 2002. Precise estimate of fundamental in-vivo MT parameters in human brain in clinically feasible times. Magn. Reson. Imaging 20, 721–731.

Silver, N.C., Good, C.D., Barker, G.J., MacManus, D.G., Thompson, A.J., Moseley, I.F., McDonald, W.I., Miller, D.H., 1997. Sensitivity of contrast enhanced MRI in multiple sclerosis. Effects of gadolinium dose, magnetization transfer contrast and delayed imaging. Brain 120, 1149–1161.

Sled, J.G., Pike, G.B., 2000. Quantitative interpretation of magnetization transfer in spoiled gradient echo MRI sequences. J. Magn. Reson. 145, 24–36.

Sled, J.G., Pike, G.B., 2001. Quantitative imaging of magnetization transfer exchange and relaxation properties in vivo using MRI. Magn. Reson. Med. 46, 923–931.

Sled, J.G., Levesque, I., Santos, A.C., Francis, S.J., Narayanan, S., Brass, S.D., Arnold, D.L., Pike, G.B., 2004. Regional variations in normal brain shown by quantitative magnetization transfer imaging. Magn. Reson. Med. 51, 299–303.

Symms, M.R., Boulby, P.A., Barker, G.J., 2003. Cross-modality registration: validation and application in magnetisation transfer imaging. Proceedings of the 11th Scientific Meeting and Exhibition of ISMRM, Toronto, p. 1050.

Tanabe, J.L., Vermathen, M., Miller, R., Gelinas, D., Weiner, M.W., Rooney, W.D., 1998. Reduced MTR in the corticospinal tract and normal T2 in amyotrophic lateral sclerosis. Magn. Reson. Imaging 16, 1163–1169.

Tofts, P.S., Cercignani, M., Tozer, D.J., Symms, M.R., Davies, G.R., Ramani, A., Barker, G.J., 2005. Quantitative magnetization transfer mapping of bound protons in multiple sclerosis. Magn. Reson. Med. 53, 492–493 (Erratum to Magn. Reson. Med. 50, 83–91, 2003).

Tozer, D., Ramani, A., Barker, G.J., Davies, G.R., Miller, D.H., Tofts, P.S., 2003. Quantitative magnetization transfer mapping of bound protons in multiple sclerosis. Magn. Reson. Med. 50, 83–91.

Venkatesan, R., Lin, W., Haacke, E.M., 1998. Accurate determination of spin-density and T1 in the presence of RF-field inhomogeneities and flip-angle miscalibration. Magn. Reson. Med. 40, 592–602.

Wolff, S.D., Balaban, R.S., 1989. Magnetization transfer contrast (MTC) and tissue water proton relaxation in vivo. Magn. Reson. Med. 10, 135–144.

Woods, R.P., Grafton, S.T., Watson, J.D., Sicotte, N.L., Mazziotta, J.C., 1998. Automated image registration: I. General methods and intrasubject, intramodality validation. J. Comput. Assist. Tomogr. 22, 139–152.

Yarnykh, V.L., 2002. Pulsed Z-spectroscopic imaging of cross-relaxation parameters in tissues for human MRI: theory and clinical applications. Mag. Reson. Med. 47, 929–939.

Yarnykh, V.L., Yuan, C., 2004. Cross-relaxation imaging reveals detailed anatomy of white matter fiber tracts in the human brain. NeuroImage 23, 409–424.